Superlattices and Microstructures 81 (2015) 151–160

Contents lists available at ScienceDirect

Superlattices and Microstructures

journal homepage: www.elsevier.com/locate/superlattices

Ultrasound-assisted preparation and characterization of β-Bi_2O_3 nanostructures: Exploring the photocatalytic activity against rhodamine B

Yashar Azizian-Kalandaragh [a,*], Farzad Sedaghatdoust-Bodagh [a], Aziz Habibi-Yangjeh [b]

[a] Department of Physics, University of Mohaghegh Ardabili, Ardabil, Iran
[b] Department of Chemistry, University of Mohaghegh Ardabili, Ardabil, Iran

ARTICLE INFO

Article history:
Received 19 November 2014
Received in revised form 18 December 2014
Accepted 22 December 2014
Available online 7 February 2015

Keywords:
Bismuth oxide
Ultrasonic irradiation
Nanostructures
UV–visible spectroscopy
Photocatalytic activity

ABSTRACT

Bismuth based oxide (β-Bi_2O_3) and mixed oxide/hydroxide nanostructures were prepared by ultrasound-assisted method in an aqueous solution. The prepared nanostructures were characterized by X-ray diffraction (XRD), energy dispersive analysis of X-rays (EDX), Fourier transformed-infrared (FT-IR) spectroscopy, scanning electron microscopy (SEM), and UV–visible absorption spectroscopy. The results revealed that the as-prepared product was crystallized in mixed phase and it converts to pure β-Bi_2O_3 by thermal treatments at 300 °C for 60 min. The band gap values for the mixed bismuth oxide/hydroxide and bismuth oxide nanostructures were 3.62 and 3.66 eV, respectively. The EDX spectrum shows that the bismuth oxide nanostructures are completely pure. The FT-IR spectrum of the products clearly demonstrates disappearance of BiO–H bonds during the thermal treatment. Photocatalytic activity of β-Bi_2O_3 nanostructures for degradation of rhodamine B, as a dye pollutant, was investigated under UV illumination.

* Corresponding author. Tel.: +98 45 33511893.
E-mail address: azizian@uma.ac.ir (Y. Azizian-Kalandaragh).

http://dx.doi.org/10.1016/j.spmi.2014.12.038
0749-6036/

1. Introduction

The preparation and characterization of nanostructured materials has been an intense field of research due to their potential applications in different technologies and interesting physiochemical properties [1–7]. Bismuth oxide is an important semiconductor material which has been used widely in the fields of catalysis [8,9], functional ceramics [10–13], optical materials [14], medicine [15], energy materials [16,17] and superconductor materials [18,19], owing to its special properties of wide band gap, high refractive index, photoluminescence and photoconductivity. There are six polymorphs of bismuth oxide named α-Bi_2O_3, β-Bi_2O_3, γ-Bi_2O_3, δ-Bi_2O_3, ω-Bi_2O_3 and ε-Bi_2O_3. The bismuth oxide polymorphs have significantly different electrical and optical properties [20]. It was reported that β-Bi_2O_3 is a p-type semiconductor with a band gap of about 2.4 eV [21,22]. Many methods such as high-temperature oxidation of bismuth metal [23,24], pyrolysis of bismuth compound [25,26], chemical vapor deposition (CVD) [27,28], sol–gel process [29], magnetron sputtering deposition [30], crystallization in glass matrix [31], template-based heat treatment [32], room temperature chemical solution route [33,34], metalorganochemical vapor deposition [35], one step aqueous method [36], thermal evaporation [37], surfactant-assisted hydrothermal synthesis [38], simple two-step solution phase approach [39] and ultrasound-assisted method [40], have been developed for preparation of bismuth oxide nanomaterials. Nano and micro-structures with anisotropic shapes and morphologies and high surface to volume ratio are aseptically attractive due to their higher photocatalytic activity [41,42]. The previously reported preparation methods are mainly limited to the formation of low-dimensional Bi_2O_3 nanostructures with 1D or 2D. However, among them, ultrasound-assisted method is very simple and has evident advantages due to good compositional control, low equipment cost and lower crystallization temperature. In the present work, we report the ultrasound-assisted method for preparation of β-Bi_2O_3 nanostructures. The ultrasound-assisted methods involve ultrasound irradiation of the precursor during synthesis. Ultrasound irradiation has been used extensively to produce novel materials with interesting properties. Because of the immense physical and chemical effects of ultrasonic waves in solutions, by using this method we can produce materials with novel properties. β-Bi_2O_3 has been reported to be a good candidate for heterogeneous photocatalysis. Despite considerable reports on the photocatalytic activity of Bi_2O_3 in visible and UV ranges, most of them are quite inconsistent and contradictory [43–45].

The main goal of this work is to synthesis a novel structure of β-Bi_2O_3 owing a feature that provides a considerable photocatalytic activity. This activity will be studied through degradation of rhodamine B in an aqueous solution under UV irradiation.

2. Experimental

2.1. Preparation of β-Bi_2O_3 nanostructures

All of the reactants and solvents were analytical grade and were used without any further purification. The experimental procedures are as follows: aqueous solution of bismuth nitrate (0.2 M) was prepared by dissolving of 1.94 g of the salt in 20 mL of double distilled water at pH = 1. This solution was irradiated with a high intensity ultrasonic at room temperature for 1 h using Dr. Heilscher ultrasound processor (UP200H Germany, 14 mm diameter Ti horn, 200 W/cm^2, 24 kHz). During the sonication of the reaction mixture, the temperature was increased to 80 °C as measured by mercury thermometer. The prepared suspension was centrifuged to get the precipitate out and washed three times using double distilled water and ethanol to remove the unreacted reagents and dried in an oven at 60 °C for 24 h. To convert the as-prepared $Bi(OH)_3$ nanostructures to β-Bi_2O_3, the as-prepared powders were annealed at 300 °C for 1 h in open air.

2.2. Instruments

The X-ray diffraction (XRD) patterns of products were recorded on a Philips X'pert X-ray diffractometer with Cu Kα radiation (λ = 1.54056 Å) employing a scanning step of 0.02° S^{-1}, in 2θ range from

20° to 80°. Surface morphologies were studied using the LEO1430 VP scanning electron microscope (SEM) with 15 and 18 kV accelerating voltages. The purity of the products were obtained by energy dispersive analysis of X-rays (EDX) on the same SEM. UV–vis absorption spectra of the samples were obtained using a Shimadzu spectrophotometer (Japan, model 1650). Fourier transform-infrared (FT-IR) spectra were obtained using Perkin Elmer Spectrum RX I apparatus. Thermal analyses were done using a thermogravimetric apparatus (model: Linseis, STA PT-1000).

2.3. Photocatalysis experiments

Photocatalysis experiments were performed in a cylindrical Pyrex reactor with about 400 mL capacity. The reactor was provided with water circulation arrangement to maintain the temperature at 25 °C. The solution was magnetically stirred and continuously aerated by a pump to provide oxygen and complete mixing of the reaction solution. A UV Osram lamp with 125 W was used as UV source. The lamp was fitted on the top of the reactor. Prior to illumination, a suspension containing 0.1 g of the nanostructures and 250 mL of RhB was continuously stirred in the dark for 30 min, to attain adsorption equilibrium. Samples were taken from the reactor at regular intervals and centrifuged to remove the photocatalyst before analysis by spectrophotometer at 554 nm corresponding to maximum absorption wavelength of RhB.

3. Results and discussion

3.1. Characterization of the nanostructure

Fig. 1(a) shows the XRD pattern of the as-prepared sample after ultrasonic irradiation for 60 min. This pattern represents diffraction peaks corresponding to mixtures of bismuth oxides (β-Bi_2O_3 and Bi_4O_7) and bismuth hydroxide. After annealing the as-prepared sample at 300 °C for 60 min, the mixture completely converts to β-Bi_2O_3 (Fig. 1(b)). Hence, it is clear that under high intensity ultrasonic irradiation for 60 min and post-annealing at 300 °C for 60 min, β-Bi_2O_3 simply was formed. No additional peaks were observed in post-annealed sample, confirming the formation the pure phase β-Bi_2O_3. The average crystallite size of β-Bi_2O_3 nanostructures was calculated using Debye–Scherer's equation [13]:

$$D = 0.94\lambda/\beta\cos\theta \tag{1}$$

where D is the average crystallite size, λ is the X-ray wavelength, β is the full-width at half maxima of the prominent peak and θ is the diffraction angle corresponding to the peak. The calculated size for β-Bi_2O_3 nanostructures is less than 23 nm.

The purity of the nanostructures was studied by EDX technique and the results are shown in Fig. 2. It is evident that the product is completely pure and the peaks correspond to Bi and O elements with an average atomic percentage ratio of about 25:75 are observed. The elemental analysis confirms the presence of corresponding elements in non-stoichiometric percentage.

Fig. 3(a) and (b) shows the FT-IR spectra of the as-prepared sample after ultrasonic irradiation for 60 min and final bismuth oxide nanostructures, respectively. The broad absorption band around 3450 cm^{-1} corresponds to the O–H stretching vibration of adsorbed water molecules on the samples [46]. The peak at 3505 cm^{-1} is related to BiO–H stretching vibration in the as-prepared sample which completely disappeared after the annealing process (Fig. 3(b)) [47]. The peaks at 814, 833 and 1037 cm^{-1} are also correspond to the stretching of bismuth oxide material [48].

The optical absorption of the as-prepared sample and β-Bi_2O_3 nanostructures were measured using UV–visible spectroscopy and the results are shown in Fig. 4(a) and (b). For crystalline semiconductor, the optical absorption near the band edge follows the equation $(\alpha h\nu)^{1/n} = A(h\nu - E_g)$, where α, ν, E_g and A are the absorption coefficient, the light frequency, the band gap and a constant, respectively [49]. The exponent n depends on the type of transition. $n = 1/2, 2, 3/2$ and 3 corresponding to allowed direct, allowed indirect, forbidden direct and forbidden indirect, respectively [50] . Taking $n = 1/2$, we have calculated the direct optical band gap from $(\alpha h\nu)^{1/n}$ vs. $h\nu$ plot (inset of Fig. 4(a) and (b)) by

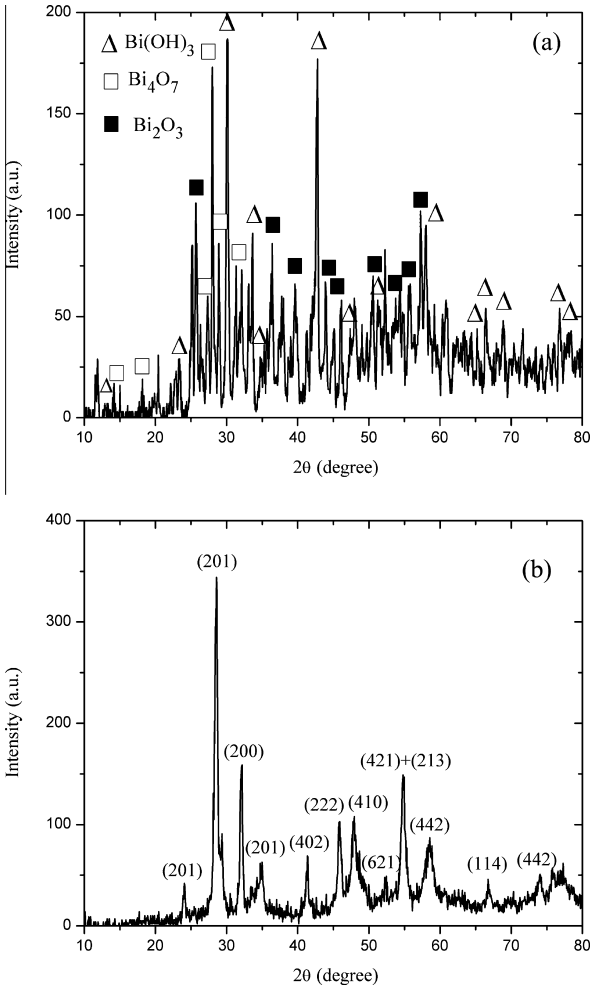

Fig. 1. X-ray diffraction patterns for (a) as-prepared sample after 60 min ultrasonic irradiation and (b) β-Bi_2O_3.

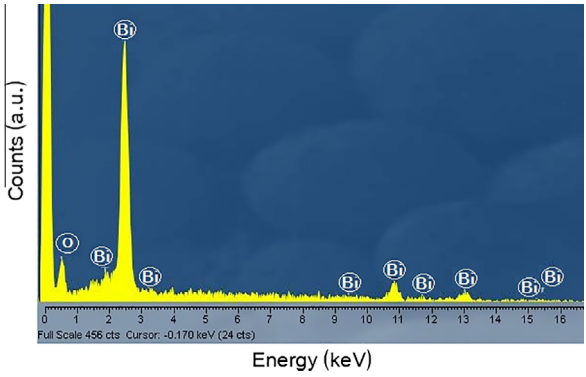

Fig. 2. EDX spectrum for β-Bi_2O_3 nanostructures.

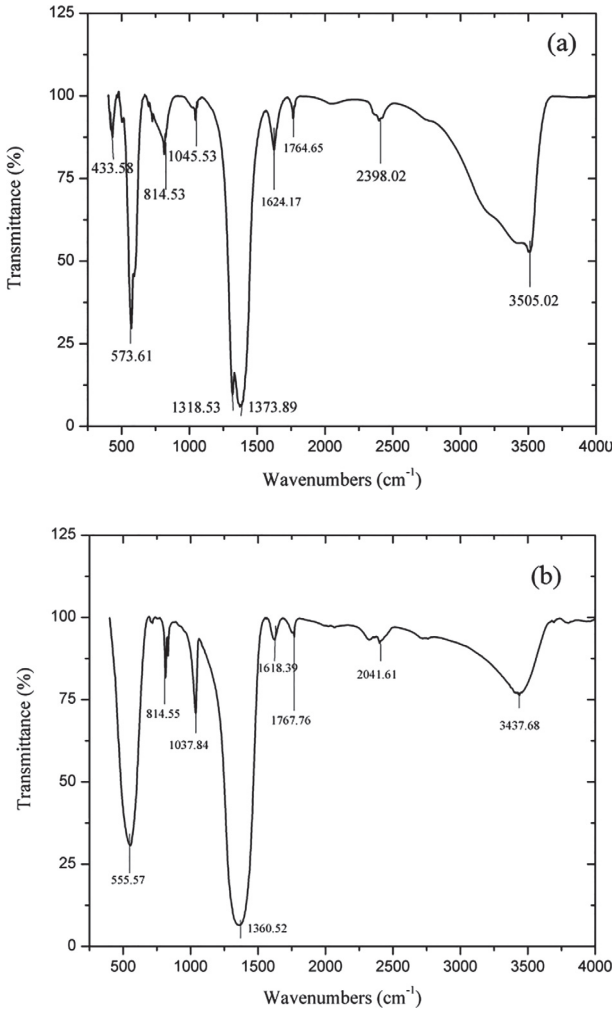

Fig. 3. FT-IR spectra of (a) as-prepared sample after 60 min ultrasonic irradiation and (b) β-Bi_2O_3.

extrapolating the linear portion of the graph to *hv* axis. The calculated band gaps for the as-prepared sample and β-Bi_2O_3 nanostructures are about 3.62 and 3.66 eV, respectively. Compared to the bulk β-Bi_2O_3, the nanostructures show a blue-shift of about 1.26 eV as a result of quantum confinement effect. When the particle radius falls below the excitonic Bohr radius, the band gap energy is widened, leading to a blue shift in the optical properties [51].

Fig. 5(a) and (b) presents SEM images for as-prepared sample and β-Bi_2O_3 nanostructures. As can be seen, both of them have a similar rectangular cubic-like morphology containing polydispersive structures. In the case of β-Bi_2O_3 nanostructures, it is clear that very small nanostructures have been formed on the rectangular cubes. The formation of these types of nanostructures could increase the effective area of the nanostructure, which can be so helpful in photocatalytic processes. The formation mechanism and the shape of the products depend on the nucleation, evolution from the nuclei to seeds, then evolution from seeds to nanostructures and finally agglomeration processes. Also these parameters will be controlled by some physical and chemical parameters such as: pH, temperature, and preparation technology. In the case of present work, we synthesized a particular shape of Bi_2O_3

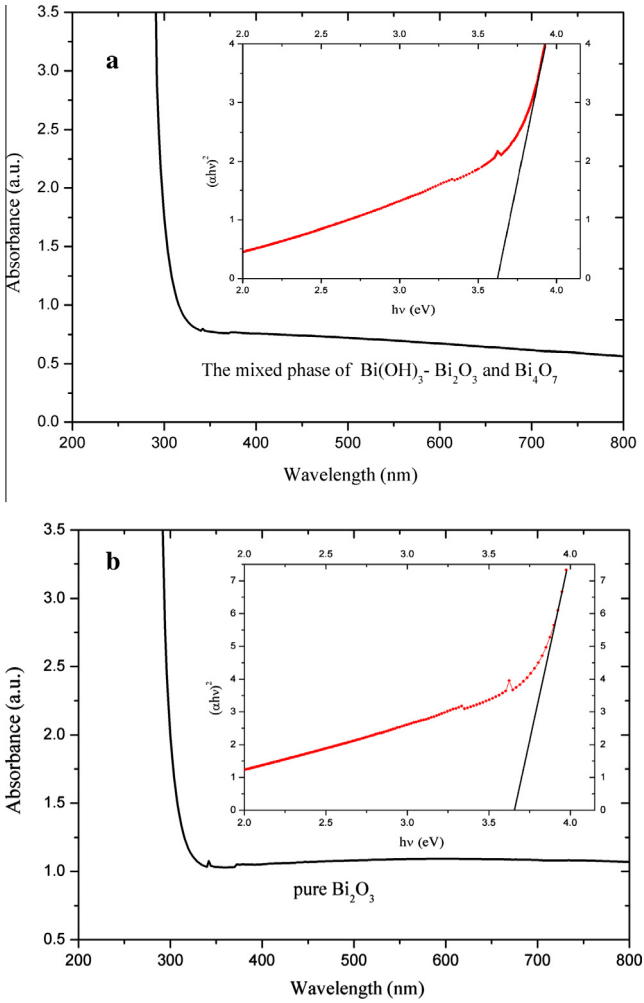

Fig. 4. UV–visible of (a) as-prepared sample after 60 min ultrasonic irradiation (mixed phase of $Bi(OH)_3$–Bi_2O_3 and Bi_4O_7) and (b) pure β-Bi_2O_3.

using a typical preparation technology that shows good results in photocatalytic reactions. As we mentioned above, the product exhibits relatively high blue-shift in the absorption edge, confirming quantum confinement effect and also high surface to volume ratio, which increases the effective band gap of the semiconductor. Moreover, it is evident from SEM image (Fig. 5(b)) that the surface of each cube consists of very small nanometer sized particles which agglomerated in the form of micron sized cubes. Although, the SEM image of bismuth oxide product does not clearly show the individual nano-sized structures, due to the limitations of the SEM apparatus, but the above explained XRD results confirmed that the crystallite size was pretty small (less than 23 nm) so that a rather considerable blue-shift occurred in the optical absorption due to strong confinement of the electrons in a small volume.

3.2. Photocatalytic activity of β-Bi_2O_3 nanostructures

Photocatalytic activity of β-Bi_2O_3 nanostructures was studied by degradation of RhB under UV irradiation at 25 °C (Fig. 6). As can be seen, the degradation of the dye on the nanostructures completely

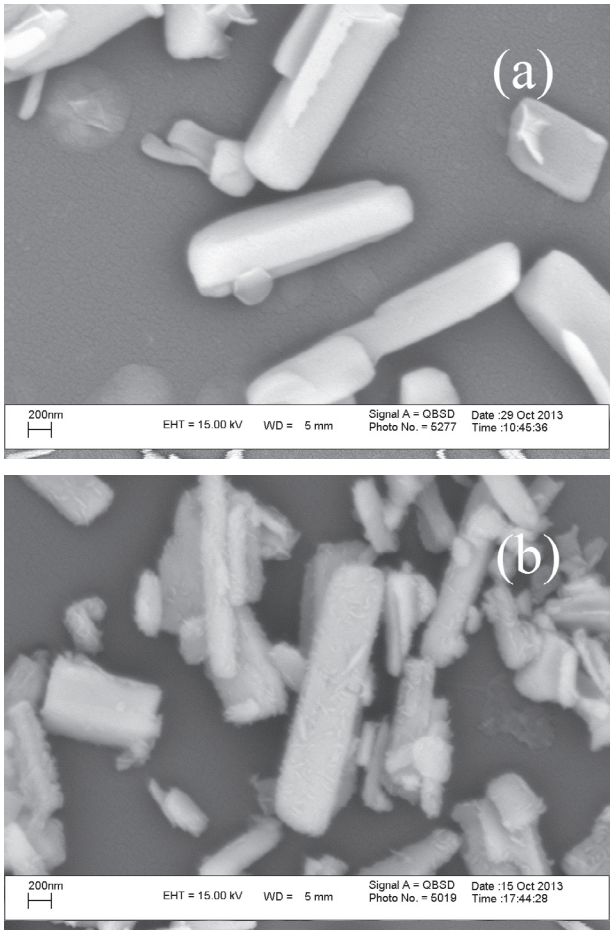

Fig. 5. SEM images for (a) as-prepared sample after 60 min ultrasonic irradiation and (b) β-Bi_2O_3.

takes place at 180 min. But, without applying UV irradiation (dark experiment), about 20% of RhB was adsorbed on the nanostructures after 240 min. In presence of the light and without using the nanostructures (photolysis experiment), only about 10% of RhB molecules were degraded after irradiation for 240 min. Therefore, under UV irradiation, decrease of RhB in the solution containing the nanostructures can be mainly assigned to photocatalytic degradation reaction. The observed first-order rate constant of the degradation reaction on the nanostructures is 13.0×10^{-3} min^{-1} [52].

Heterogeneous photocatalysis reactions closely related to the reactive species produced during the process. The role of these species in the degradation reaction was investigated by measuring the performance of various scavengers after UV irradiation for 180 min (Fig. 7). The degradation percentage, without using any scavenger and in presence of 2-PrOH is 100%. However, with addition of benzoquinone and KI, the degradation percentages decrease to 70.3 and 50.9%, respectively. Benzoquinone, KI and 2-PrOH are scavengers for $\cdot O^{2-}$, h^+ and ·OH, respectively [53,54]. As can be seen, 2-PrOH has not any effect on the degradation percentage. Moreover, the effect of KI is greater than that of benzoquinone. Therefore, it can be concluded that the effects of holes and O^{2-} species in RhB degradation on the nanostructures are higher than that of hydroxyl radical.

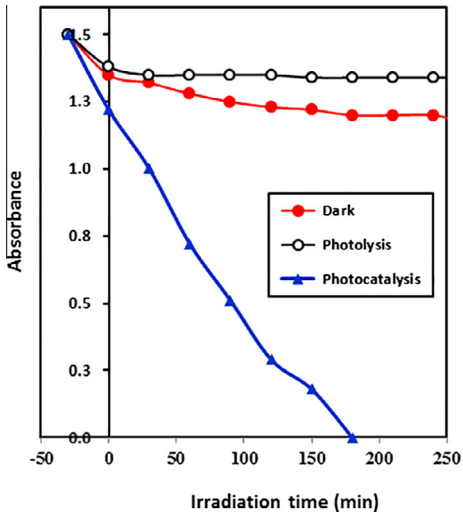

Fig. 6. Photodegradation of RhB on β-Bi_2O_3 nanostructures along with dark and photolysis data.

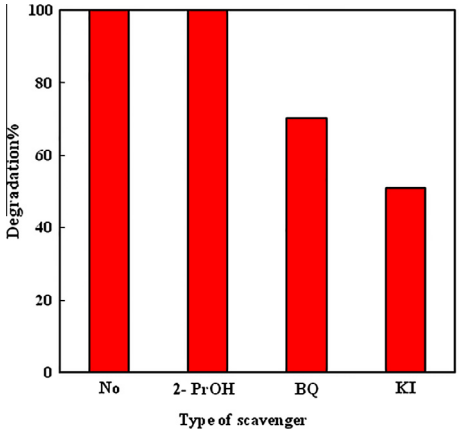

Fig. 7. Degradation percentage of RhB on the β-Bi_2O_3 nanostructures in presence of various scavengers.

4. Conclusion

Ultrasound-assisted method was successfully applied for aqueous preparation of β-Bi_2O_3 nanostructures. The products were characterized by different techniques. The XRD patterns showed that the sample crystallized in mixed phases and converted to β-Bi_2O_3 structure after thermal treatment at 300 °C. The elemental analysis using EDX technique confirmed formation of pure β-Bi_2O_3 nanostructures. The SEM images showed that very small nanostructures have been formed on the rectangular cubes of the β-Bi_2O_3 nanostructures. FT-IR spectra of the samples revealed that the peak at 3505 cm^{-1} is related to BiO–H stretching vibration in the as-prepared sample which completely disappeared after the annealing process. Compared to the bulk β-Bi_2O_3, the nanostructures show a blue-shift of 1.26 eV as a result of quantum confinement effect. Photocatalytic activity of the prepared nanostructures for degradation of RhB under UV irradiation was also studied. The effects of various

scavengers demonstrated that the effects of holes and $\cdot O_2^-$ species in degradation of RhB on the nanostructures are higher than that of hydroxyl radical.

Acknowledgements

The authors thank the supports by the physical chemistry lab of UMA and one of the authors (Farzad) thanks to Mr. M. Azadi for his helps and patience during performing this work.

References

[1] R. Zhuo, Y. Wang, D. Yan, S. Li, Y. Liu, F. Wang, One-step synthesis and excellent microwave absorption of hierarchical tree-like ZnO nanostructures, Mater. Lett. 117 (2014) 34–36.
[2] Y. Azizian-Kalandaragh, A. Khodayari, Z. Zeng, C.S. Garoufalis, S. Baskoutas, L.C. Gontard, Strong quantum confinement effect in SnS nanocrystals produced by ultrasound-assisted method, J. Nanopart. Res. 15 (2013).
[3] H. Zeynali, H. Akbari, R.K. Ghasabeh, Y. Azizian-Kalandaragh, S.M. Hosseinpour-Mashkani, Effect of Zn addition on the reduction of the ordering of FePt nanoparticles, J. Supercond. Novel Mag. 26 (2012) 713–717.
[4] X. Liu, Y. Gao, R. Jin, H. Luo, P. Peng, Y. Liu, Scalable synthesis of Si nanostructures by low-temperature magnesiothermic reduction of silica for application in lithium ion batteries, Nano Energy 4 (2014) 31–38.
[5] K.-S. Kang, Fabrication of large area nanostructures with surface modified silica spheres, Superlattices Microstruct. 67 (2014) 17–24.
[6] M.S. Fuhrer, J. Nygard, L. Shih, M. Forero, Y.G. Mazzoni, H.J. Choi, Crossed nanotube junctions, Science 288 (2000) 494.
[7] P.D. Yang, H.Q. Yan, S. Mao, R. Russo, J. Johnson, R. Saykally, Controlled growth of ZnO nanowires and their optical properties, Adv. Funct. Mater. 12 (5) (2002) 323.
[8] J. Sheng-Ming, T. Mo-Tang, Y. Wei-Jun, Preparation of catalyst for ammoxidation of propylene in chlorination salts systems – catalytic activity rating of Bi containing catalyst, J. Cent. South Univ. Technol: Nat. Sci. 32 (4) (2001) 247–250.
[9] Y. Han-Pei, F. Yi-Ning, L. Ming, X. Bo-Ian, C. Yi, Structure and catalytic properties of Bi−Mo composite oxide catalyst for selective oxidation of propane, Chin. J. Catal. 60 (6) (2002) 1006–1010.
[10] Z. Lazerevic, B.D. Stonavic, J.A. Varela, An approach to analyzing synthesis, structure and properties of bismuth titanate ceramics, J. Sci. Sintering 37 (3) (2005) 199–216.
[11] P. Nikonika, S. Vlademir V, Synthesis and structural characterization of Ce-doped bismuth titanate, J. Mater. Res. Bull. 44 (4) (2009) 860–864.
[12] K. Laurent, G.Y. Wang, S. Tusseau-Nenez, Y. Leprince-Wang, Structure and conductivity studies of electrodeposited δ-Bi_2O_3, Solid State Ionics 178 (33-34) (2008) 1735–1739.
[13] S. Zong-Ping, X. Guo-Xing, Y. Wei-Shen, Progress in bismuth-contained mixed conducting oxide membranes, J. Inorg. Mater. 16 (1) (2001) 23–31.
[14] T. Hasegava, T. Nagashima, N. Sugimoto, Determination of nonlinear coefficient and group-velocity-dispersion of bismuth-based high nonlinear optical fiber by four-wave-mixing, Opt. Commun. 281 (4) (2008) 782–787.
[15] Y. Nan, S. Hong-zhe, Biocoordination chemistry of bismuth: recent advances, Coord. Chem. Rev. 25 (17–20) (2007) 2354–2366.
[16] J. Zhi-yi, Z. Lei, C. Li-li, X. Chang-rong, Bismuth oxide-coated (La, Sr)MnO_3 cathodes for intermediate temperature solid oxide fuel cells with yttria-stabilized zirconia electrolytes, J. Electrochem. Acta 54 (11) (2009) 3059–3065.
[17] A. Smirinova, S. Sarat, N. Sammes, Bismuth oxide doped candia-stabilized zirconia electrolyte for the intermediate temperature solid oxide fuel cells, J. Power Sources 160 (2) (2006) 892–896.
[18] L. Yu-Bao, L. Liang-Zhen, Xi. Li-Ye, Development of bismuth-base high temperature superconducting DC cable, Physics 30 (7) (2001) 389–391.
[19] M.V. Makarov, P.E. Kazin, Y.D. Teryakov, M. Jansen, M. Reissner, W. Steiner, Zr, Hf, Mo and W-containing oxide phases as pinning additives in Bi-2212 superconductor, Physica C 419 (1) (2005) 61–69.
[20] M. Mehring, From molecules to bismuth oxide-based materials, Coord. Chem. Rev. 251 (2007) 974–1006.
[21] Y. Qiu, M. Yang, H. Fan, Y. Zuo, Y. Shao, Y. Xu, X. Yang, S. Yang, Nanowire of α- and β-Bi_2O_3: phase-selective synthesis and application in photocatalysis, CrytEngComm 13 (2010) 1843–1850.
[22] X. Xiao, R. Hu, C. Lio, C. Xing, C. Qian, X. Zuo, J. Nan, L. Wang, Facile large-scale synthesis of β-Bi_2O_3 nanospheres as a highly efficient photocatalyst for the degradation of acetaminophen under visible light irradiation, Appl. Catal. B: Environ. 140–141 (2013) 433–443.
[23] H. Han-Xiang, X. QiuKe-Qiang, X. Guo-Fu, Preparation of nanometer δ and β-bismuth trioxide by vacuum vapor-phase oxidation, Trans. Nonferrous Met. Soc. China 16 (1) (2006) 173–177.
[24] K.S. Martirosyan, L. Wang, A. Vicent, D. Luss, Synthesis and performance of bismuth trioxide nanoparticles for high energy gas generator use, Nanotechnology 20 (40) (2009) 405–412.
[25] J. Kruger, P. Winkler, E. Luderiz, M. Luck, H.U. Wolf, Bismuth, bismuth alloys, and bismuth compounds, Ullmann's Encyclopedia of Industrial Chemistry, Wiley–VCH Verlag GmbH, Weinheim, Germany, 2000.
[26] L. Madier, S.E. Pratsinis, Bismuth oxide nano-particles by flame spray pyrolysis, J. Am. Ceram. Soc. 85 (7) (2002) 1713–1718.
[27] H. Jung, C.F. Feldmann, Polymediated synthesis of submicrometer Bi_2O_3 particles, J. Mater. Sci. 36 (1) (2001) 297–299.
[28] B.M. Ataev, A.M. Bagamadova, A.M. Djabrailov, Highly conductive and transparent Ga-doped epitaxial ZnO films on sapphire by CVD, Thin Solid Films 260 (1) (1995) 19.
[29] W. He, W. Qin, X. Wu, X. Ding, L. Chen, Z. Jiang, The photocatalytic properties of bismuth oxide films prepared through the sol–gel method, Thin Solid Films 515 (13) (2007) 5362–5365.

[30] B. Sirota, J. Reyes-Cuellar, P. Kohli, L. Wang, M.E. McCarroll, S.M. Aouadi, Bismuth oxide photocatalytic nanostructures produced by magnetron sputtering deposition, Thin Solid Films 520 (19) (2012) 6118–6123.
[31] S.M. Abo-Naf, R.L. Elwan, G.M. Elkomy, Crystallization of bismuth oxide nano-crystallites in a SiO_2–PbO–Bi_2O_3 glass matrix, J. Non-Cryst. Solids 358 (5) (2012) 964–968.
[32] B.J. Yang, M.S. Mo, H.M. Hu, C. Li, X.G. Yang, Q.W. Li, Y.T. Qian, A rational self-sacrificing template route to β-Bi_2O_3 nanotube arrays, Eur. J. Inorg. Chem. (2004) 1785–1787.
[33] S. Iyyapushpam, S.T. Nishanthi, D. Pathinettam-Padiyan, Synthesis of room temperature bismuth oxide and its photocatalytic activity, Mater. Lett. 86 (2012) 25.
[34] X. Gou, R. Li, G. Wang, Z. Chen, D. Wexler, Room-temperature solution synthesis of Bi_2O_3 nanowires for gas sensing application, Nanotechnology 20 (49) (2009) 495501.
[35] H.W. Kim, J.H. Myung, S.H. Shim, C. Lee, Growth of Bi_2O_3 rods using a trimethylbismuth and oxygen mixture, Appl. Phys. A Mater. Sci. Process. 84 (2006) 187–189.
[36] W. Yi, Z. Jingzhe, W. Zichen, A simple low-temperature fabrication of oblique prism-like bismuth oxide via a one-step aqueous process, Colloids Surf. A; Physicochem. Eng. Aspects 377 (1-3) (2011) 409–413.
[37] X.P. Shen, S.K. Wu, H. Zhao, Q. Liu, Synthesis of single-crystalline Bi_2O_3 nanowires by atmospheric pressure chemical vapor deposition approach, Physica E 39 (2007) 133–136.
[38] H. Lu, S. Wang, L. Zhao, B. Dong, Z. Xu, J. Li, Surfactant-assisted hydrothermal synthesis of Bi2O3nano/microstructures with tunable size, RSC Adv. 2 (8) (2012) 3374.
[39] P. Arun-Prakash, Y. Singying, C. Shen-Ming, Preparation and characterization of bismuth oxide nanoparticles-multiwalled carbon nanotube composite for the development of horseradish peroxidase based H_2O_2 biosensor, Talanta 87 (2011) 15–23.
[40] P.D. Dimple, Roy, A.K. Tyagi, Dual function of rare earth doped nano Bi_2O_3: white light emission and photocatalytic properties, Dalton Trans. 41 (2012) 10238.
[41] V. Taghvaei, A. Habibi-Yangjeh, M. Behboudnia, Simple and low temperature preparation and characterization of CdS nanoparticles as a highly efficient photocatalyst in presence of a low-cost ionic liquid, J. Iran. Chem. Soc. (2010) 75–176.
[42] S. Eftekhari, A. Habibi-Yangjeh, Sh. Sohrabnezhad, Application of AlMCM-41 for competitive adsorption of methylene blue and rhodamine B: thermodynamic and kinetic studies, J. Hazard. Mater. 178 (2010) 349–355.
[43] L. Zhang, W. Wange, J. Yang, Z. Chen, W. Zhang, L. Zhou, S. Liu, Sonochemical synthesis of nanocrystallite Bi_2O_3 as a visible-light-driven photocatalyst, Appl. Catal. 308 (2006) 105–110.
[44] K. Brezesinski, R. Ostermann, P. Hartman, J. Perlich, T. Brezesinski, Exceptional photocatalytic activity of ordered mesoporous β-Bi_2O_3 thin films and electrospun nanofiber mats, Chem. Mater. 22 (2010) 3079–3085.
[45] T. Saison, N. Chemin, C. Chan, O. Durupthy, V. Ruaux, L. Mariey, F. Maug, P. Beaunier, J.P. Jolivet, Bi_2O_3, $BiVO_4$, and Bi_2WO_6: impact of surface properties on photocatalytic activity under visible light, Phys. Chem. C 115 (2011) 5657–5666.
[46] M. Bosca, L. Pop, G. Borodi, P. Pascuta, E. Culea, XRD and FTIR structural investigations of erbium-doped bismuth-lead silver glasses and glass ceramics, J. Alloys Compd. 479 (2009) 579–582.
[47] F. He, J. Wang, D.W. Deng, Effect of Bi_2O_3 on structure and wetting studies of Bi_2O_3–ZnO–B_2O_3 glasses, J. Alloys Compd. 509 (2011) 6332–6336.
[48] M. Ristic, S. Popovic, S. Music, Formation and properties of $Cd(OH)_2$ and CdO particles, Mater. Lett. 58 (2004) 2494–2499.
[49] L. Zhang, W. Wang, J. Yang, Z. Chen, W. Zhang, L. Zhou, S. Liu, Sonochemical synthesis of nanocrystallite Bi_2O_3 as a visible-light-driven photocatalyst, Appl. Catal. A: Gen. 308 (2006) 105–110.
[50] A. Abdolahzadeh Ziabari, F.E. Ghodsi, G. Kiriakidis, Correlation between morphology and electro-optical properties of nanostructured CdO thin films: influence of Al doping, Surf. Coat. Technol. 213 (2012) 15–20.
[51] A. Abdolahzadeh Ziabari, F.E. Ghodsi, Growth, characterization and studying of sol–gel derived CdS nanoscrystalline thin films incorporated in polyethyleneglycol: effects of post-heat treatment, Sol. Energy Mater. Sol. Cells 105 (2012) 249–262.
[52] M. Rezaei, A. Habibi-Yangjeh, Simple and large scale refluxing method for preparation of Ce-doped ZnO nanostructures as highly efficient photocatalyst, Appl. Surf. Sci. 265 (2013) 591–596.
[53] L.S. Zhang, K.H. Wong, H.Y. Yip, C. Hu, J.C. Yu, C.Y. Chan, P.K. Wong, Effective photocatalytic disinfection of *E. coli* K-12 using AgBr–Ag–Bi_2WO_6 nanojunction system irradiated by visible light: the role of diffusing hydroxyl radicals, Environ. Sci. Technol. 44 (2010) 1392–1398.
[54] G.T. Li, K.H. Wong, X.W. Zhang, C. Hu, J.C. Yu, R.C.Y. Chan, P.K. Wong, Degradation of acid orange 7 using magnetic AgBr under visible light: the roles of oxidizing species, Chemosphere 76 (2009) 1185–1191.